Intermolecular Locking Design of Red Thermally Activated Delayed Fluorescence Molecules for High-Performance Solution-Processed Organic Light-emitting Diodes

Jibiao Jin,[a] Wuji Wang,[a] Peiran Xue,[a] Qingqing Yang,[a] He Jiang,[a] Ye Tao,[a] Chao Zheng,[a]* Guohua Xie,[b]* Wei Huang,[a, c] Runfeng Chen[a]*

[a] Key Laboratory for Organic Electronics and Information Displays & Jiangsu Key Laboratory for Biosensors, Institute of Advanced Mate-rials (IAM), Nanjing University of Posts & Telecommunications, 9 Wenyuan Road, Nanjing 210023, China.

[b] Sauvage Center for Molecular Sciences, Hubei Key Lab on Organic and Polymeric Optoelectronic Materials, Department of Chemistry, Wuhan University, Wuhan, 430072, China.

[c] Frontiers Science Center for Flexible Electronics (FSCFE), Shaanxi Institute of Flexible Electronics (SIFE) & Shaanxi Institute of Biomed-ical Materials and Engineering (SIBME), Northwestern Polytechnical University (NPU), 127 West Youyi Road, Xi'an 710072, China.

*Corresponding authors (email: iamczheng@njupt.edu.cn; guohua.xie@whu.edu.cn; iamrchen@njupt.edu.cn)

1. Background information

Table S1. A brief summary of recent solution-processed red TADF OLEDs on turn-on voltage (in V), current efficiency (CE, in cd A^{-1}), external quantum efficiency (EQE, in %) and EQE roll off at 1000 cd m^{-2}.

Compound	Turn-on Voltage	Maximum Efficiency		Roll-off	References
		CE	EQE		
NAI_R3	7.0	28.3	22.5	86%	[1]
NAI_R2	4.0	19.6	11.5	66%	[1]
TAT-DBPZ	3.2	29.7	15.4	47%	[2]
TAT-FDBPZ	3.0	14.0	9.2	19%	[2]
tDBBPZ-DPXZ	4.5	12.8	10.1	>57%	[3]
FDQPXZ	-	-	9.0	32%	[4]
4t-BuCzTTR	4.7	13.0	6.2	87%	[5]
PFDMPE-R01	10.2	9.3	4.07	>22%	[6]
PFDMPE-R05	9.8	10.3	5.62	>82%	[6]
PFDMPE-R07	8.6	8.3	4.64	>82%	[6]
PFDMPE-R10	6.4	4.8	2.90	>75%	[6]
BTZPP	3.5	6.2	3.4	-	[7]
red-1b	-	1.22	1.75	-	[8]
DTPAB	4.4	16.4	8.2	57%	**This work**
DPhCzB	4.7	17.0	6.7	9%	**This work**
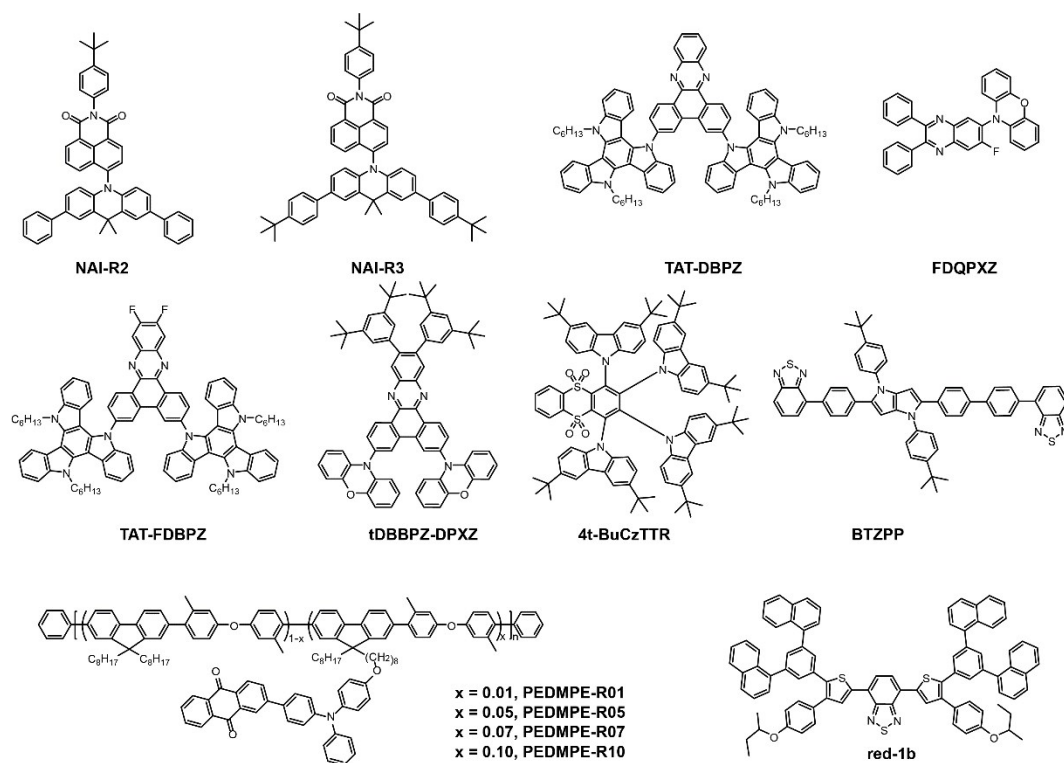
Scheme S1. Molecular structures of the representative solution-processible red TADF materials reported recently.

2. Synthesis and characterization

Materials. Chemical reagents, unless otherwise specified, were purchased from Energy Chemical, Acros, or Alfa Aesar, and used without further purification. Manipulations involving air-sensitive reagents were performed in an atmosphere of dry argon.

Instruments. ^{1}H and ^{13}C-nuclear magnetic resonance (NMR) spectra were recorded on a Bruker Ultra Shield Plus 400 MHz instrument with CDCl$_3$ or DMSO-d_6 as the solvent and tetramethylsilane (TMS) as the internal standard. High resolution mass spectrum (HRMS) was obtained on a LCT Premier XE (Waters) HRMS spectrometry.
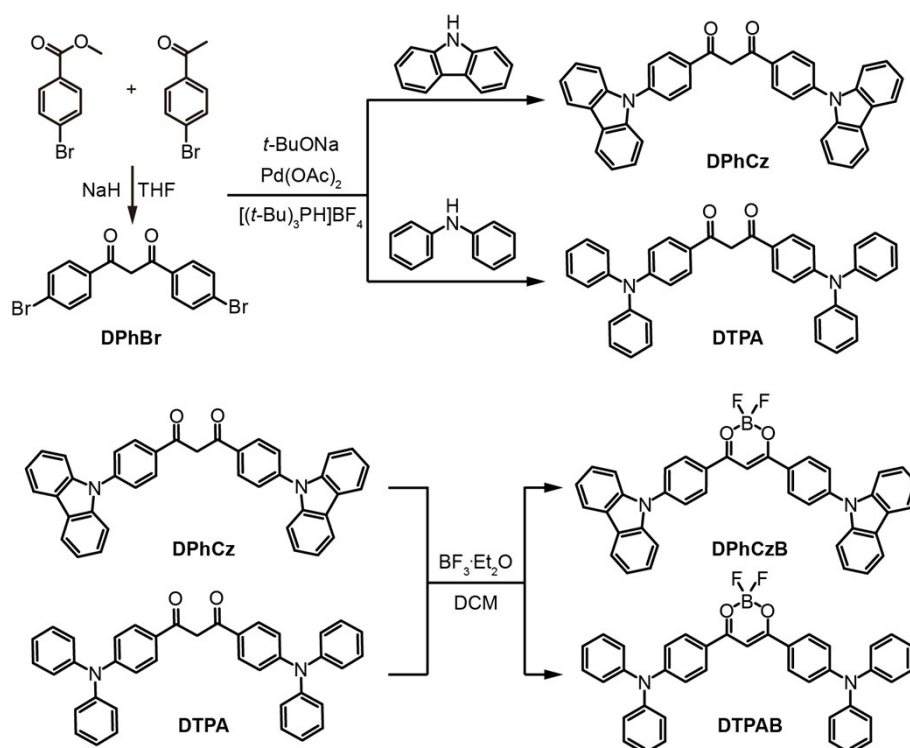
Scheme S2. Synthetic route for preparing the thermally activated delayed fluorescent (TADF) molecules with intermolecular locking.

Synthesis of 1,3-bis(4-bromophenyl)propane-1,3-dione (DPhBr)

A mixture of a sodium hydride in oil dispersion (60%, 0.53 g, 22 mmol) and methyl 4-bromobenzoate (2.3 g, 10 mmol) in 30 mL of dry tetrahydrofuran (THF) was heated to 60°C. On continuous stirring of the above mixture, 1-(4-bromophenyl)ethan-1-one (2.0 g, 10 mmol) in 20 mL of dry THF was added dropwise. And the reaction temperature was held at 60 °C for 1 day. Then, the reaction mixture was poured into water and neutralized with hydrochloric acid. The resulting precipitate was collected and recrystallized from ethanol to give pale yellow needlelike crystals. Yield: 70%.

Synthesis of 1,3-bis(4-(9H-carbazol-9-yl)phenyl)propane-1,3-dione (DPhCz)

DPhBr (0.50 g, 1.31 mmol), carbazole (0.55 g, 3.28 mmol), tBuONa (0.31 g, 3.28 mmol), Pd(OAc)$_2$ (15 mg, 0.07 mmol) and [(tBu)$_3$PH]BF$_4$ (57 mg, 0.20 mmol) were dissolved in a degassed toluene solution (50 mL). The resultant mixture was stirred at 110℃ for 24 hours under dry argon atmosphere to complete the reaction. Then, the solution was cooled to room temperature, washed with water (30 mL), and extracted with dichloromethane (3×30 mL). The organic layers were collected, combined and dried by anhydrous Na$_2$SO$_4$ and purified through column chromatography. Yield: 0.50 g of yellow powder (68%). ^{1}H NMR (400 MHz, DMSO-d_6): δ= 8.55 (d, J = 8.0 Hz, 4H), 8.30 (d, J = 8.0 Hz, 4H), 7.91 (d, J = 8 Hz, 4H), 7.57 (d, J = 8 Hz, 4H), 7.49 (t, J = 16 Hz, 4H), 7.35 (t, J = 16 Hz, 4H), 7.64 (s, 1H).

Synthesis of 1,3-bis(4-(diphenylamino)phenyl)propane-1,3-dione (DTPA)

DTPA was prepared under the identical synthetic conditions described in the preparation of **DPhCz**, using **DPhBr** (0.50 g, 1.31 mmol), diphenylamine (0.56 g, 3.28 mmol), tBuONa (0.31 g, 3.28 mmol), Pd(OAc)$_2$ (15 mg, 0.07 mmol) and [(tBu)$_3$PH]BF$_4$ (57 mg, 0.20 mmol). Yield: 0.55 g of yellow powder (75%). ^{1}H NMR (400 MHz, DMSO-d_6): δ= 7.98 (d, J = 8.0 Hz, 4H), 7.43-7.38 (m, J = 20 Hz, 9H), 7.21-7.15 (d, J = 24 Hz, 12H), 6.93 (d, J = 4 Hz, 4H).

Synthesis of difluoroboron 1,3-bis(4-(9H-carbazol-9-yl)phenyl)propane-1,3-dione (DPhCzB)

To a solution of **DPhCz** (0.50 g, 0.90 mmol) in 20 mL CH$_2$Cl$_2$ was added BF$_3$·Et$_2$O (0.35 g, 2.70 mmol) under a dry argon atmosphere. The mixture was refluxed overnight. Then, the reaction was quenched by cooling to room temperature and washing with water (30 mL). The resulting mixture was extracted with CH$_2$Cl$_2$ (3×30 mL) and the organic layers were collected and dried with anhydrous Na$_2$SO$_4$. After removing the solvent by vacuum-rotary evaporation, the solid residue was purified by column chromatography (silica gel, 3:1 v/v, PE/CH$_2$Cl$_2$). Yield: 0.35 g of red powder (65%). ^{1}H NMR (400 MHz, DMSO-d_6): δ= 8.32 (d, J = 8.0 Hz, 4H), 8.20 (d, J = 8.0 Hz, 4H), 7.81 (d, J = 8 Hz, 4H), 7.56 (d, J = 8 Hz, 4H), 7.48 (t, J = 16 Hz, 4H), 7.36 (t, J = 16 Hz, 4H), 7.06 (s, 1H). ^{13}C NMR (100 MHz, CDCl$_3$): δ= 181.80, 144.51, 139.82, 130.84, 129.83, 126.58, 126.47, 124.28, 121.24, 120.64, 109.86, 93.42. HRMS (ESI): *m/z* calcd. for C$_{39}$H$_{25}$BF$_2$N$_2$O$_2$Na ([M+Na]$^+$), 625.1875; found, 625.1877.
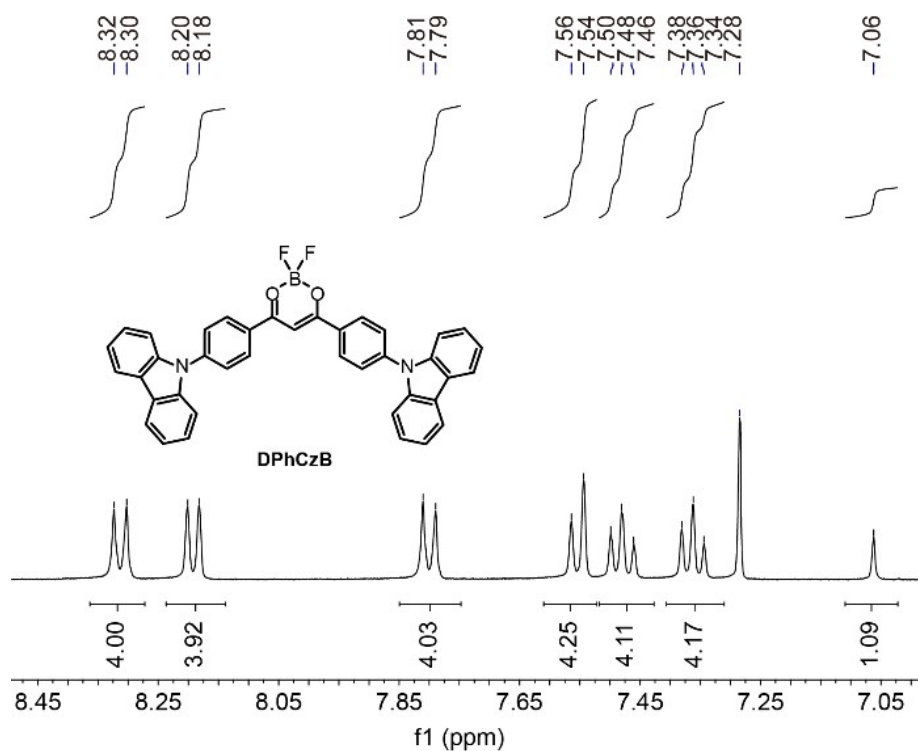
Figure S1. ^{1}H NMR spectrum of **DPhCzB** in CDCl$_3$.
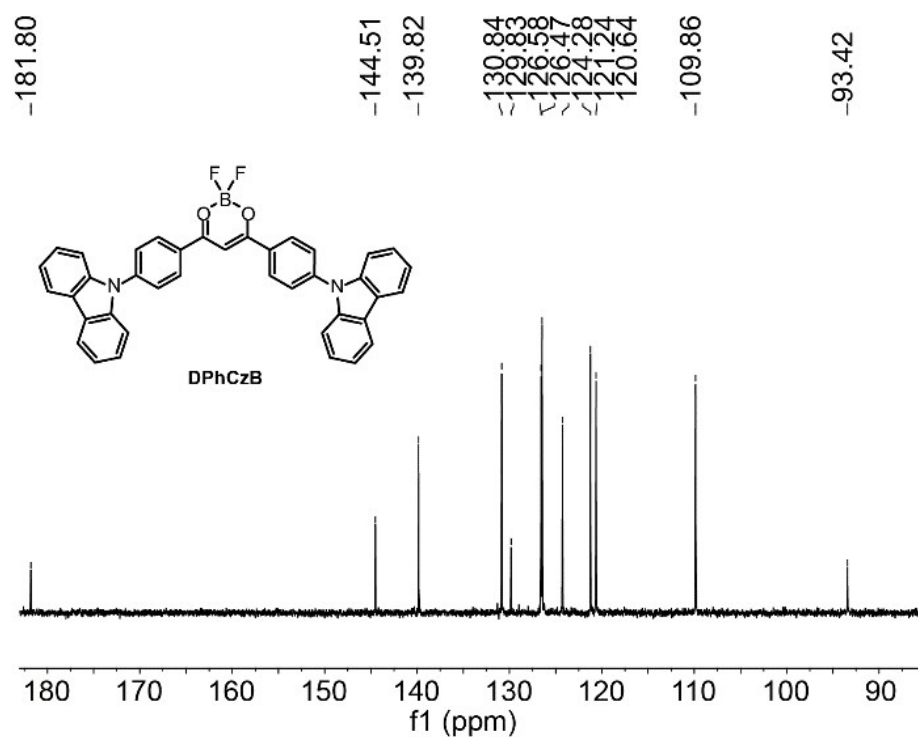
Figure S2. ^{13}C NMR spectrum of **DPhCzB** in CDCl$_3$.
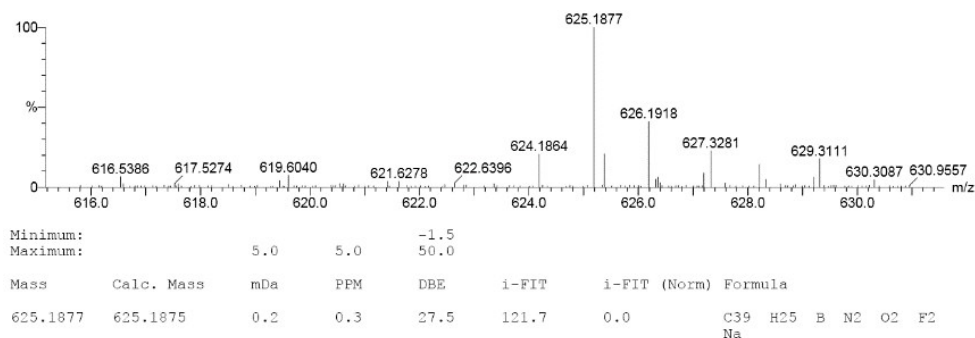
Figure S3. HRMS of **DPhCzB**.

Synthesis of difluoroboron 1,3-bis(4-(diphenylamino)phenyl)propane-1,3-dione (DTPAB)

DTPAB was prepared under the identical synthetic conditions described in the preparation of **DPhCzB**, using DTPA (0.50 g, 0.90 mmol) and $BF_3 \cdot Et_2O$ (0.35 g, 2.70 mmol). Yield: 0.40 g of red powder (74%). ^{1}H NMR (400 MHz, DMSO-d_6): δ= 8.14 (d, J = 8.0 Hz, 4H), 7.46 (t, J = 16 Hz, 9H), 7.31-7.25 (m, J = 24 Hz, 12H), 6.89 (d, J = 12 Hz, 4H). ^{13}C NMR (100 MHz, CDCl$_3$): δ= 178.92, 153.63, 145.74, 130.42, 129.83, 126.49, 125.56, 123.44, 118.92, 90.98. HRMS (ESI): *m/z* calcd. for $C_{39}H_{25}BF_2N_2O_2$ (M), 606.2290; found, 606.2294.
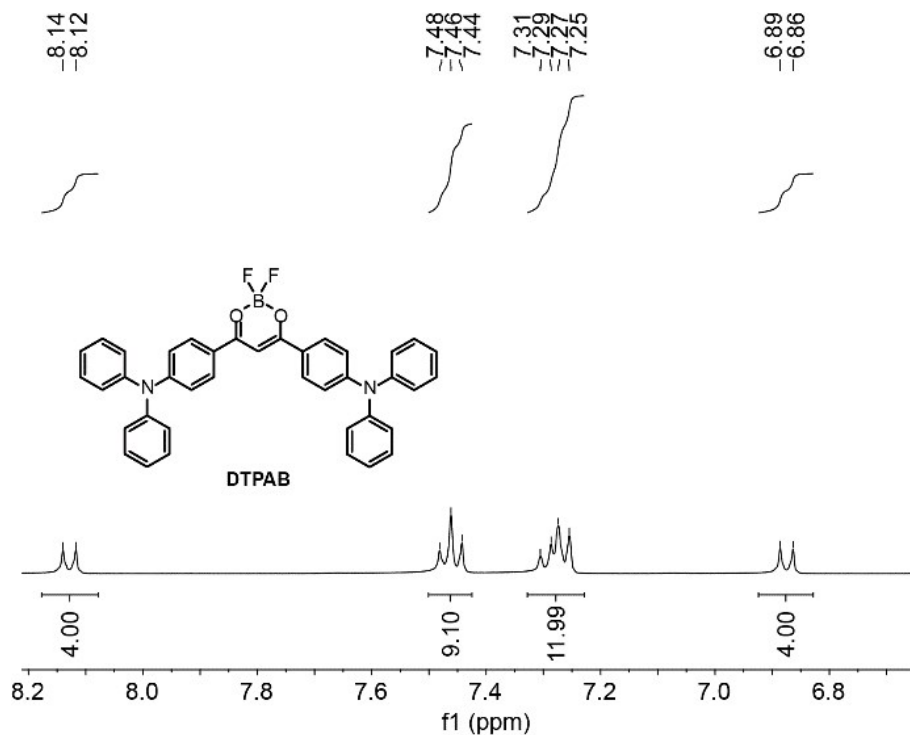
Figure S4. ^{1}H NMR spectrum of **DTPAB** in DMSO-d_6.
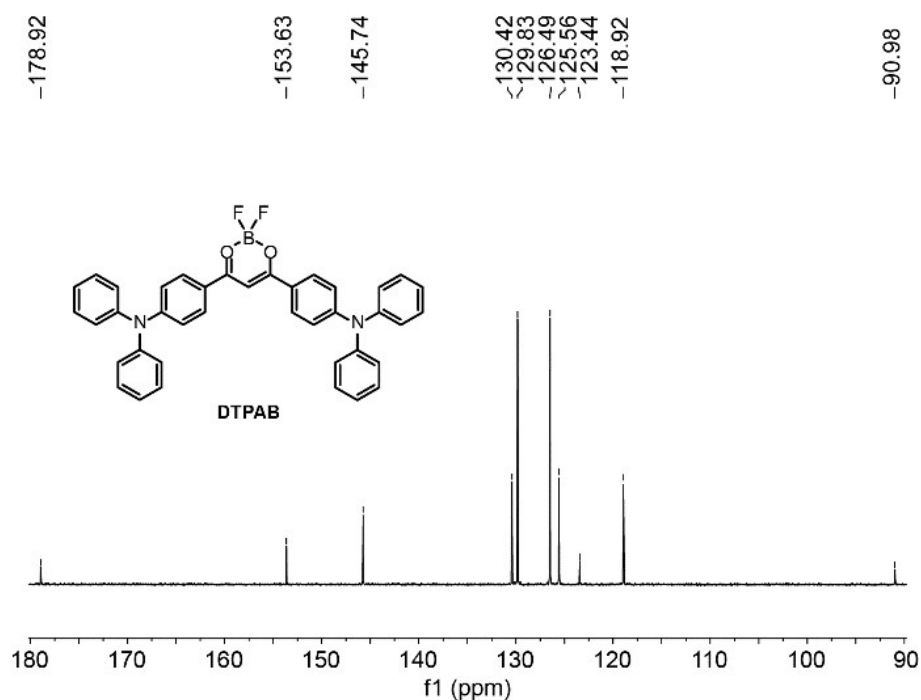
Figure S5. ^{13}C NMR spectrum of **DTPAB** in CDCl$_3$.

Mass	Calc. Mass	mDa	PPM	DBE	i-FIT	i-FIT (Norm)	Formula
606.2294	606.2290	0.4	0.7	26.0	143.6	0.0	C39 H29 B N2 O2 F2
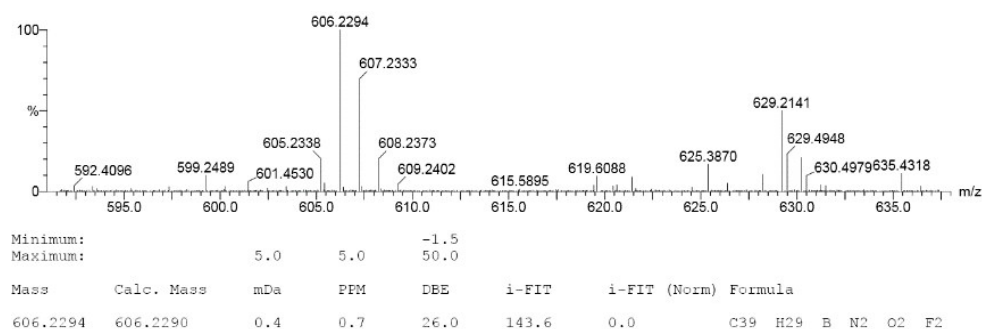
Figure S6. HRMS of **DTPAB**.

3. Single crystal analysis

Single crystal of **DPhCzB** was grown by slow evaporation of a mixed CH$_2$Cl$_2$ and PE (petroleum ether) solution at room temperature. The data of the single crystal structure were collected on a Bruker SMART APEX (II)-CCD at 298 K. Crystal structures were analyzed by Mercury 1.4 software. The CCDC number for **DPhCzB** is 2021616. The crystallographic data were summarized in **Table S2**.

Table S2. Crystallographic data of **DPhCzB**.

Empirical formula	$C_{39}H_{25}BF_2N_2O_2$
Formula weight (g mol^{-1})	602.45
Crystal color	red
Wavelength (Å)	0.71073
Crystal system	Orthorhombic
Space group	*Pbcn*
a (Å)	6.9869(11)
b (Å)	19.139(3)
c (Å)	22.504(4)
α (deg)	90
β (deg)	90
γ (deg)	90
V (Å^3)	3009.3(8)
Z	4
Density (g cm^{-3})	1.330
μ (mm^{-1})	0.090
T_{min}, T_{max}	0.6412, 0.7547
F(000)	1248
h_{max}, k_{max}, l_{max}	9, 23, 30
$Theta_{max}$	28.356
CCDC number	2021616

4. Thermal property, morphology and solubility investigations

Thermogravimetric analyses (TGA) were conducted on a DTG-60 Shimadzu thermal analyst system under a heating rate of 10ºC/min and a nitrogen flow rate of 50 cm^3/min. The differential scanning calorimetry (DSC) analyses were performed on a Shimadzu DSC-60A instrument under a heating rate of 10ºC/min and a nitrogen flow rate of 20 cm^3/min. The film morphology of these molecules designed by intermolecular locking strategy was investigated by atomic force microscopy (AFM) measurements, which were carried out at room temperature using a Bruker Dimension Icon AFM equipped with Scanasyst-Air peak force tapping mode AFM tips from Bruker. The solubilities of **DPhCzB** and **DTPAB** in different organic solvents of toluene, dichloromethane (DCM), trichloromethane (TCM) and THF were tested and the results were summarized in Table S3.
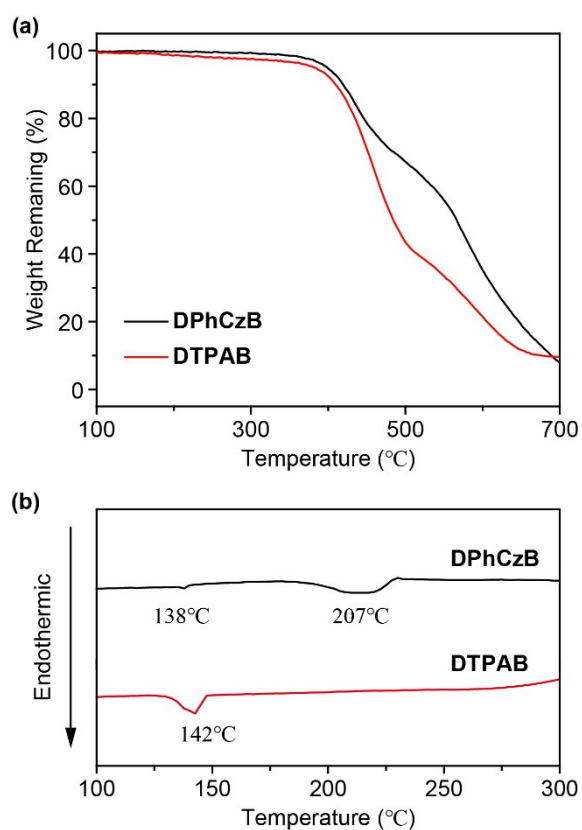
Figure S7. (a) TGA and (b) DSC curves of **DPhCzB** and **DTPAB**.
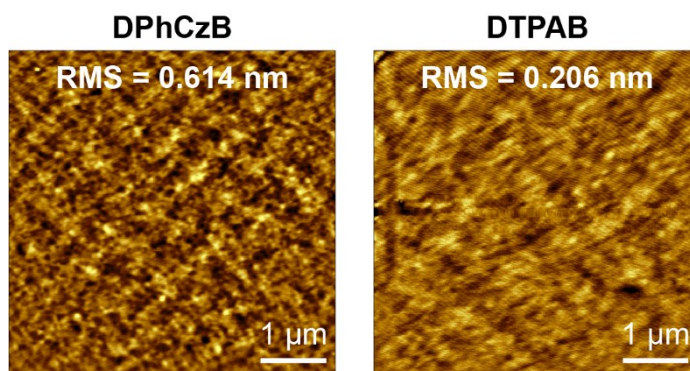
Figure S8. AFM height images of the spin-coated thin films of **DPhCzB** and **DTPAB** on ITO substrates.

Table S3. Solubility test of **DPhCzB** and **DTPAB** (in mg mL^{-1}).

Compound	Toluene	DCM	TCM	THF
DPhCzB	40	70	86	80
DTPAB	120	230	245	228

5. Photophysical properties

Ultraviolet/visible (UV/Vis) absorption and photoluminescence (PL) spectra of the molecules with intermolecular locking were recorded on a Lambda 650 S Perkin Elmer UV/VIS spectrophotometer and Edinburgh FLS 980 fluorescence spectrophotometer, respectively. For fluorescence lifetime measurements, a picosecond pulsed light emitting diode (EPLED-380, wavelength: 377 nm; pulse width: 947.7 ps) was used. The phosphorescence spectra in dilute toluene were obtained using an Edinburgh FLS 980 fluorescence spectrophotometer at 77 K in a dewar vessel with a 5 ms delay time after excitation using a microsecond (μs) flash lamp. The absolute photoluminescence quantum yields (PLQY) were measured using an integrating sphere. The lifetimes of the luminescence were figured out by fitting the luminescent intensity decay curve (I(t)) with a multi-exponential decay function of

$$I(t) = \sum_i A_i e^{-\frac{t}{\tau_i}}$$

where A_i and τ_i represent the amplitudes and lifetimes of the individual PL components in multi-exponential decay profiles, respectively.
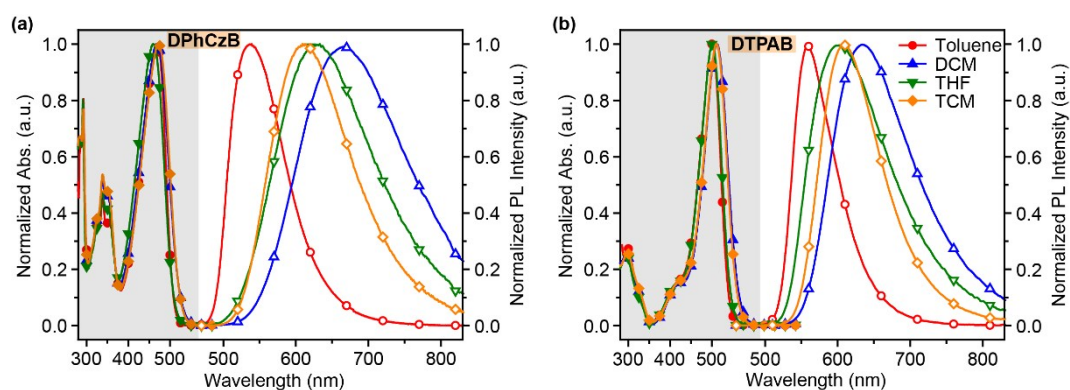
Figure S9. UV-vis absorption (solid symbols) and photoluminescence spectra (open symbols) of (a) **DPhCzB** and (b) **DTPAB** in toluene, DCM, THF and TCM at room temperature.
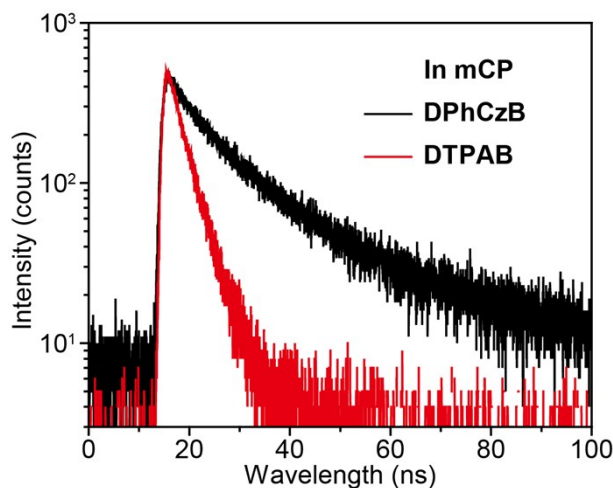
Figure S10. Transient PL decay curves of **DPhCzB** or **DTPAB** (5 wt%) doped in 1,3-di(9H-carbazol-9-yl)benzene (*m*CP)　film at room temperature. The excitation wavelength is 380 nm.

6. Computational methods

Density functional theory (DFT) calculations were performed on Gaussian 09 revision D.01 package to theoretically study their molecular geometries and electronic properties[9]. Molecular structures were fully optimized by the Becke's three-parameter exchange functional along with the Lee-Yang-Parr correlation functional (B3LYP) at the standard split valence plus polarization function 6-31G(d) basis set for the most stable single molecular state on the ground state (S_0). Nonbonding covalent interaction (NCI) analyses were adopted to investigate the intermolecular interactions using Multiwfn version 3.7 software based on the B3LYP/6-31G(d) optimized molecular structures at S_0. NCI isosurface plots were performed with color scaling that the dark blue color represents attractive interactions, while dark red color represents repulsive interactions. All the plotted isosurfaces were demonstrated with reduced density gradient (RDG) of 0.5 and $-0.5 < \text{sign}(\lambda_2)\rho < 0.5$, where $\text{sign}(\lambda_2)$ means the sign of the second largest eigenvalue of Hessian and ρ represents the electron density.
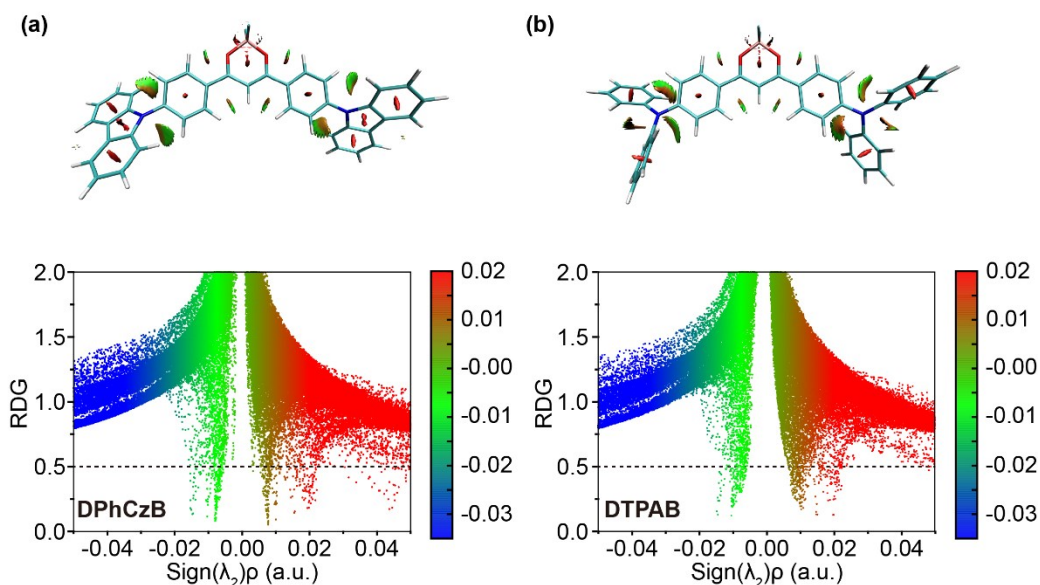
Figure S11. Reduced density gradient (RDG) versus sign(λ_2)ρ with the view of the RDG isosurface based on the optimized single molecular structures of (a) DPhCzB and (b) DTPAB.

Optimized molecular geometry   Molecular geometry in crystal
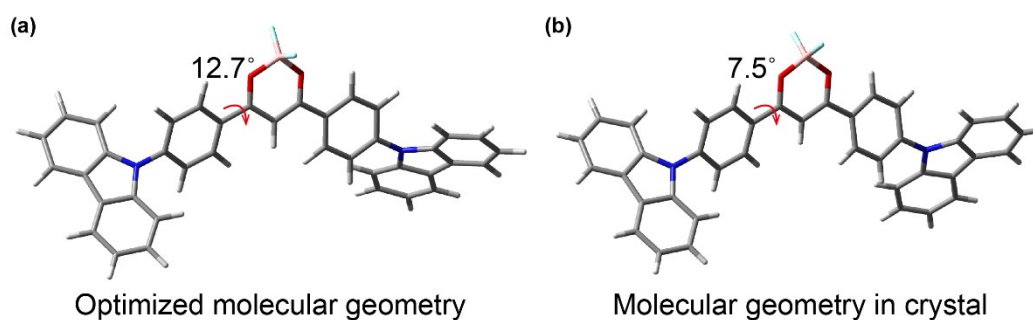
Scheme S3. (a) Theoretically optimized molecular geometry of **DPhCzB**. (b) Molecular geometry in **DPhCzB** crystal.

7. Electrochemical properties

Cyclic voltammetry (CV) measurements were performed at room temperature on a CHI660E system in a typical three-electrode cell with a working electrode (glass carbon), a reference electrode Ag/Ag$^+$ referenced against ferrocene/ferrocenium (FOC), and a counter electrode (Pt wire). The electrochemical experiments were carried out in an acetonitrile solution of Bu$_4$NPF$_6$ (0.1 M) at a sweeping rate of 100 mV s^{-1}. The highest occupied molecular orbital (HOMO) energy levels (E_{HOMO}) of the materials deposited as thin films on the surface of the working electrode were measured based on the reference energy level of ferrocene (4.8 eV below the vacuum) according to Equation S1:

$$E_{HOMO} = -\left[E_{onset}^{Ox} - E_{(Fc/Fc^+)} + 4.8\right]eV \tag{S1}$$

where $E_{(Fc/Fc+)}$ is the onset oxidative voltage of FOC vs Ag/Ag+ and is the onset potential of the oxidation wave. The lowest unoccupied molecular orbital (LUMO) energy level (E_{LUMO}) was estimated by adding the optical band-gap (E_g) to the corresponding HOMO energy level as in Equation S2[10]:

$$E_{LUMO} = \left[E_{HOMO} + E_g \right] eV \qquad\qquad\qquad\text{(S2)}$$
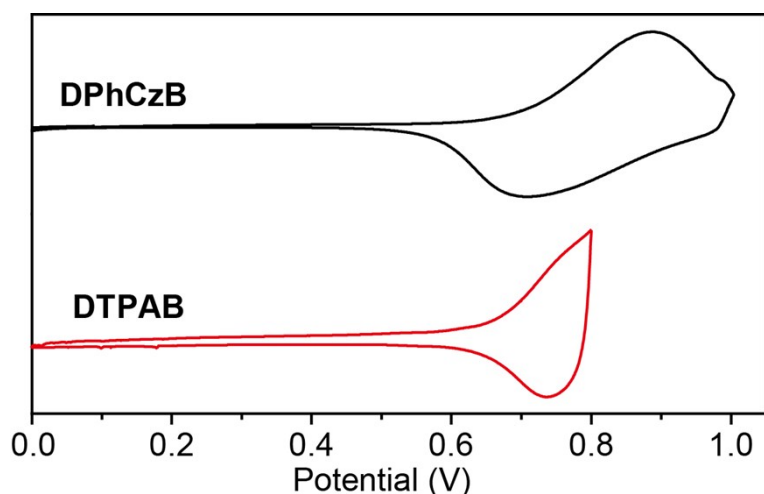
Figure S12. CV curves of **DPhCzB** and **DTPAB** thin films deposited on the surface of glass carbon electrode.

8. Devices fabrication and measurements

The hole-injection material of poly(3,4-ethylenedioxythiophene): poly (styrenesulfonic acid) (PEDOT: PSS) was purchased from H.C. Starck. The electron-transporting material of 1,3,5-tri(m-pyrid-3-yl-phenyl)-benzene (TmPyPB), electron-injection material of 8-Hydroxyquinolinolato-lithium (Liq), the host material of 1,3-di(9H-carbazol-9-yl)benzene (*m*CP) and the exciton-block material of (oxybis(2,1-phenylene))bis(diphenylphosphine oxide) (DPEPO) were from Nichem Fine Technology Co. Ltd. All the above-mentioned materials were used as-received without further purification.

Red TADF organic light emitting diode (OLED) devices were fabricated in the following procedure. The patterned ITO glass substrates were ultrasonically cleaned with detergent, alcohol, acetone, and deionized water for 30 min respectively, and then dried at 120°C in a vacuum oven for more than one hour. After ultraviolet (UV)-ozone treating for 15 min, a 40 nm PEDOT: PSS was spin coated on the ITO substrate and dried at 120°C in a vacuum oven for 15 min. Then, the emissive layers (EMLs) were spin-coated on the top of PEDOT: PSS from chlorobenzene and annealed using a hot plate at 80°C for 20 min to remove residual solvents. After that, the samples were transferred to a thermal evaporator chamber. DPEPO (10 nm), TmPyPB (50 nm), Liq (1 nm), and Al (100 nm) were deposited subsequently by thermal evaporation under a pressure of 5×10^{-4} Pa. The thickness of these vacuum-deposited layers was monitored using a spectroscopic ellipsometry (α-SE, J.A. Wollam Co. Inc.). The active area of the devices is 4.4 mm^2. The devices without encapsulation were measured immediately after

fabrication at room temperature under ambient atmosphere conditions. The luminance-current-voltage (L-J-V) characteristics of the devices were recorded by a combination of a Keithley source-meter (model 2602) and a calibrated luminance meter. Electroluminescence (EL) spectra were obtained using a spectra-scan PR735 spectrophotometer. The external quantum efficiency (EQE) was achieved according to Equation S3[11].

$$EQE = \frac{\pi e \eta_{cd/A} \int \lambda p(\lambda) d\lambda}{hc K_m \int p(\lambda) \Phi(\lambda) d\lambda} \tag{S3}$$

where $\eta_{cd/A}$ is the current efficiency (cd/A); h is the Planck constant; c is the speed of light in vacuum; λ is the wavelength (nm); e is the electron charge; $p(\lambda)$ is relative electroluminescent intensity at each wavelength; $\Phi(\lambda)$ is the Commision International de l'Eclairage chromaticity (CIE) standard photopic luminous efficiency function; and K_m is a constant of 683 lm/W.
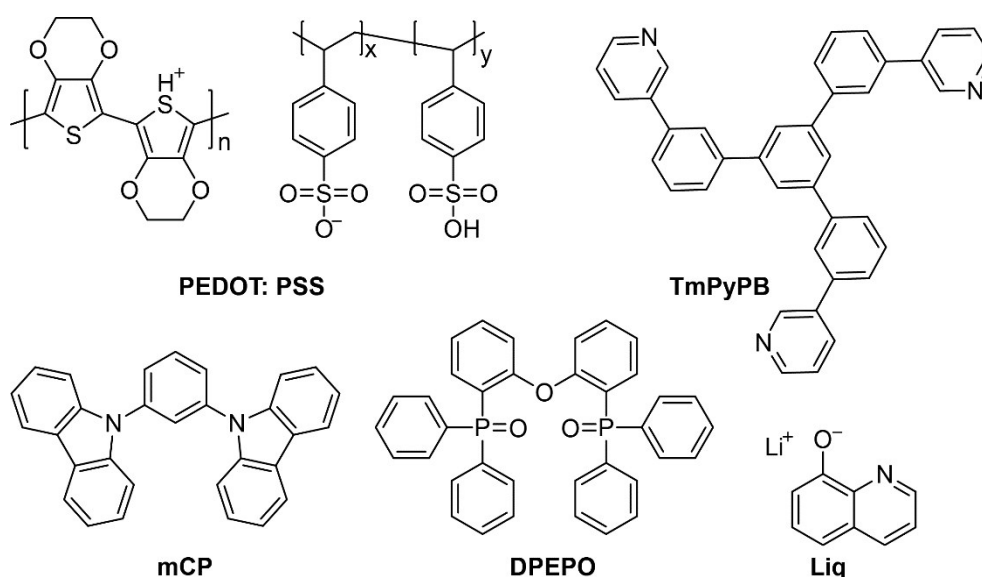
Figure S13. Molecular structures of the materials used in the OLEDs.
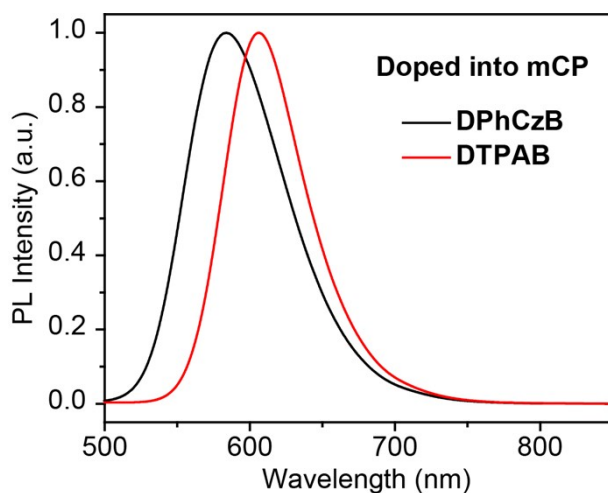
Figure S14. PL spectra of the red TADF emitters doped in *m*CP (5 wt%) films.

References:

[1] Zeng, W.; Zhou, T.; Ning, W.; Zhong, C.; He, J.; Gong, S.; Xie, G.; Yang, C. Realizing 22.5% External Quantum Efficiency for Solution-Processed Thermally Activated Delayed-Fluorescence OLEDs with Red Emission at 622 nm via a Synergistic Strategy of Molecular Engineering and Host Selection. *Adv. Mater.* **2019**, *31*, e1901404.

[2] Liu, Y.; Chen, Y.; Li, H.; Wang, S.; Wu, X.; Tong, H.; Wang, L. High-Performance Solution-Processed Red Thermally Activated Delayed Fluorescence OLEDs Employing Aggregation-Induced Emission-Active Triazatruxene-Based Emitters. *ACS Appl. Mater. Interfaces* **2020**, *12*, 30652.

[3] Chen, J. X.; Tao, W. W.; Xiao, Y. F.; Wang, K.; Zhang, M.; Fan, X. C.; Chen, W. C.; Yu, J.; Li, S.; Geng, F. X.; Zhang, X. H.; Lee, C. S. Efficient Orange-Red Thermally Activated Delayed Fluorescence Emitters Feasible for Both Thermal Evaporation and Solution Process. *ACS Appl. Mater. Interfaces* **2019**, *11*, 29086.

[4] Yu, L.; Wu, Z.; Xie, G.; Zhong, C.; Zhu, Z.; Cong, H.; Ma, D.; Yang, C. Achieving a balance between small singlet-triplet energy splitting and high fluorescence radiative rate in a quinoxaline-based orange-red thermally activated delayed fluorescence emitter. *Chem. Commun.* **2016**, *52*, 11012.

[5] Li, X.; Wang, K.; Shi, Y.-Z.; Zhang, M.; Dai, G.-L.; Liu, W.; Zheng, C.-J.; Ou, X.-M.; Zhang, X.-H. Efficient solution-processed orange-red organic light-emitting diodes based on a novel thermally activated delayed fluorescence emitter. *J. Mater. Chem. C* **2018**, *6*, 9152.

[6] Yang, Y.; Zhao, L.; Wang, S.; Ding, J.; Wang, L. Red-Emitting Thermally Activated Delayed Fluorescence Polymers with Poly(fluorene-co-3,3′-dimethyl diphenyl ether) as the Backbone. *Macromolecules* **2018**, *51*, 9933.

[7] Zhou, Y.; Zhang, M.; Ye, J.; Liu, H.; Wang, K.; Yuan, Y.; Du, Y.-Q.; Zhang, C.; Zheng, C.-J. Zhang, X.-H. Efficient solution-processed red organic light-emitting diode based on an electron-donating building block of pyrrolo[3,2-b]pyrrole. *Org. Electron.* **2019,** *65*, 110.

[8] Chen, P.; Wang, L. P.; Tan, W. Y.; Peng, Q. M.; Zhang, S. T.; Zhu, X. H.; Li, F. Delayed fluorescence in a solution-processable pure red molecular organic emitter based on dithienylbenzothiadiazole: a joint optical, electroluminescence, and magnetoelectroluminescence study. *ACS Appl. Mater. Interfaces* **2015**, *7*, 2972.

[9] G. W. T. M. J. Frisch, H. B. Schlegel, G. E. Scuseria, M. A. Robb, J. R. Cheeseman, G. Scalmani, V. Barone, G. A. Petersson, H. Nakatsuji, X. Li, M. Caricato, A. Marenich, J. Bloino, B. G. Janesko, R. Gomperts, B. Mennucci, H. P. Hratchian, J. V. Ortiz, A. F. Izmaylov, J. L. Sonnenberg, D. Williams Young, F. Ding, F. Lipparini, F. Egidi, J. Goings, B. Peng, A. Petrone, T. Henderson, D. Ranasinghe, V. G. Zakrzewski, J. Gao, N. Rega, G. Zheng, W. Liang, M. Hada, M. Ehara, K. Toyota, R. Fukuda, J. Hasegawa, M. Ishida, T. Nakajima, Y. Honda, O. Kitao, H. Nakai, T. Vreven, K. Throssell, J. A. Montgomery, Jr., J. E. Peralta, F. Ogliaro, M. Bearpark, J. J. Heyd, E. Brothers, K. N. Kudin, V. N. Staroverov, T. Keith, R. Kobayashi, J. Normand, K. Raghavachari, A. Rendell, J. C. Burant, S. S. Iyengar, J. Tomasi, M. Cossi, J. M. Millam, M. Klene, C. Adamo, R. Cammi, J. W. Ochterski, R. L. Martin, K. Morokuma, O. Farkas, J. B. Foresman, and D. J. Fox, Journal, 2016, Revision D.01.

[10] Jin, J.; Tao, Y.; Jiang, H.; Chen, R.; Xie, G.; Xue, Q.; Tao, C.; Jin, L.; Zheng, C.; Huang, W. Star-Shaped Boron-Containing Asymmetric Host Materials for Solution-Processable Phosphorescent Organic Light-Emitting Diodes. *Adv. Sci.* **2018,** *5*, 1800292.

[11] Tao, Y.; Guo, X.; Hao, L.; Chen, R.; Li, H.; Chen, Y.; Zhang, X.; Lai, W.; Huang, W. A Solution-Processed Resonance Host for Highly Efficient Electrophosphorescent Devices with Extremely Low Efficiency Roll-off. *Adv. Mater.* **2015**, *27*, 6939.